Biomaterials 232 (2020) 119676

Contents lists available at ScienceDirect

Biomaterials

journal homepage: www.elsevier.com/locate/biomaterials

Neutralizing tumor-promoting inflammation with polypeptide-dexamethasone conjugate for microenvironment modulation and colorectal cancer therapy

Sheng Ma[a,b,c], Wantong Song[a,c,**], Yudi Xu[a,c,d], Xinghui Si[a,b,c], Dawei Zhang[a,c], Shixian Lv[e], Chenguang Yang[a,c], Lili Ma[a,c], Zhaohui Tang[a,b,c], Xuesi Chen[a,b,c,*]

[a] Key Laboratory of Polymer Ecomaterials, Changchun Institute of Applied Chemistry, Chinese Academy of Sciences, Changchun, 130022, PR China
[b] University of Science and Technology of China, Hefei, 230026, PR China
[c] Jilin Biomedical Polymers Engineering Laboratory, Changchun, 130022, PR China
[d] University of Chinese Academy of Sciences, Beijing, 100039, PR China
[e] Department of Bioengineering, Molecular Engineering and Sciences Institute, University of Washington, Seattle, 98195, USA

ARTICLE INFO

Keywords:
Polypeptide
Dexamethasone
Tumor microenvironment
Anti-Inflammation

ABSTRACT

Tumor is known as “a wound that does not heal”. Tumor-promoting inflammation plays a crucial role in carcinogenesis, tumor progression, tumor metastasis, as well as chemotherapy resistance. Therefore, reducing tumor-promoting inflammation may be a key aspect in targeting the tumor microenvironment for cancer therapy. Dexamethasone (DEX), a commercial drug in the treatment of many different inflammatory diseases, can effectively inhibit the release of substances causing inflammation. However, as a corticosteroid medication, direct use of DEX results in many severe side effects. In this study, a redox and pH dual sensitive polypeptide-DEX conjugate (L–SS–DEX) was synthesized, and the L–SS–DEX dramatically increased the tumoral accumulation of DEX in murine colorectal cancer model (CT26) compared to free DEX. Importantly, at equal dose (10 mg/kg), L–SS–DEX showed superior antitumor activity over free DEX: 86% tumor suppression rate of L–SS–DEX treatment group compared to 49% of free DEX treatment group. Further analysis of the tumor tissues showed that cyclooxygenase-2 (COX-2) and α-smooth muscle actin (α-SMA) were significantly reduced after the L–SS–DEX treatment compared with control groups. In addition, the immunosuppressive microenvironment of the CT26 tumor was effectively relieved after L–SS–DEX treatment, characterized by increased $CD8^+$ T cell infiltration, increased ratio of M1 over M2 macrophages, as well as markedly decrease in regulatory T cells (Tregs) and myeloid-derived suppressor cells (MDSCs). The above results suggest that anti-inflammatory drugs hold great potential in modulating the tumor microenvironment when delivered properly, and can also result in significant tumor inhibition effects. Since dramatic amounts of anti-inflammatory drugs have been used in clinic, our results may provide improved tumor therapy options of using anti-inflammatory drugs for cancer therapy.

1. Introduction

Tumor is described as “a wound that doesn't heal”, and tumor-promoting inflammation is one of the hallmarks of cancer [1,2]. Inflammation, especially chronic inflammation, is an important cause of tumorigenesis and acts different functions accompanied with tumor progression [3,4]. It is gradually illustrated that the tumor microenvironment (TME) is constructed by not only tumor cells, but also stroma cells including endothelial cells, fibroblasts, as well as inflammatory cells [5]. Specially, certain inflammatory cells like tumor-associated macrophages (TAMs), assist tumor cell hyperplasia by secreting growth factors [6], assist angiogenesis through secreting vascular endothelial growth factor (VGEF) [7,8], promote tumor metastasis and invasion by secreting matrix metalloproteinases (MMPs) [9], and suppress adaptive immunity by secreting various immunosuppressive cytokines [10,11]. Besides, some of the inflammatory cells are reported to contribute to drug resistance [12]. As a result, immunomodulation with reducing inflammation may be an important

* Corresponding author. Key Laboratory of Polymer Ecomaterials, Changchun Institute of Applied Chemistry, Chinese Academy of Sciences, Changchun, 130022, PR China.
** Corresponding author. Jilin Biomedical Polymers Engineering Laboratory, Changchun, 130022, PR China.
E-mail address: xschen@ciac.ac.cn (X. Chen).

https://doi.org/10.1016/j.biomaterials.2019.119676
Received 28 August 2019; Received in revised form 24 November 2019; Accepted 7 December 2019
Available online 16 December 2019
0142-9612/

strategy to remodel the TME for cancer therapy.

Anti-inflammatory drugs have been applied in clinic for cancer prophylaxis. Anti-inflammatory drugs have also shown efficacy in suppressing tumor progression [13], counteracting chemoresistance [14], decreasing cancer morbidity [15], and improving the survival of cancer patients [16]. For example, non-steroidal anti-inflammatory drug (NSAIDs) aspirin was reported to reduce the incidence of several types of solid tumors including prostate cancer [17], melanoma [18] and breast cancer [19]. Steroidal anti-inflammatory drugs such as dexamethasone (DEX) has been used in combination with Venetoclax to improve the sensitivity in myeloma [20]. Besides, DEX could enhance the therapeutic effect of platinum and gemcitabine based chemotherapeutics in the treatment of colon cancer [21], lung cancer [22] and breast cancer [23]. Statins show ability to activate natural killer cells which results in tumor inhibition and tumor microenvironment modulation [24]. Despite this, NSAIDs, steroids and statins have various side effects, including kidney dysfunction [25], Cushing's syndrome [26], gastrointestinal bleeding [27], osteroporosis [28], liver dysfunction [29] and coagulopathy [30], which however hindered their full applications to cancer therapy.

Nanotechnology-based delivery systems have been widely explored in recent years in chemo-drug delivery for improving water solubility [31,32], prolonging blood circulation time [33], regulating the biological distribution [34,35] and reducing side effects [36]. Besides, nanomedicine-based immunomodulation has created enormous impact in both clinical and preclinical studies in cancer therapy [37–42]. Several attempts have been reported on the preparation of nano-formulations of anti-inflammatory drugs, and a few of them has been applied in cancer therapy [43–45]. In one study, DEX was encapsulated in long-circulating liposomes and crosslinked polymeric micelles for melanoma treatment. Although long circulating half-lives and reduced systemic side effects were observed, the nano-formulation only resulted in modest tumor suppression effect, which might be attributed to unsatisfactory drug release [46]. In another study, celecoxib was co-loaded with doxorubicin in albumin which result in enhanced antitumor efficacy of doxorubicin in non-small cell lung cancer treatment [47]. Stimulus-responsive drug delivery systems have been reported to further enhance the drug delivery efficiency by reducing unnecessary drug release at normal tissues and promoting fast release inside tumor [48]. However, stimuli-responsive drug delivery systems are still rarely reported for delivering anti-inflammatory drugs for cancer therapy. We hypothesized that the stimuli-responsive design may maximize therapeutic effects of these anti-inflammatory drugs.

To validate such hypothesis, a kind of pH and redox dual responsive polypeptide-DEX conjugate (L–SS–DEX) was developed for anti-tumor therapy and tumor microenvironment modulation (Scheme 1). Polypeptide was chosen as the backbone materials in this study due to its good biocompatibility [49], low toxicity [50] and versatile functionalization [51]. The antitumor effect of L–SS–DEX was evaluated in a murine CT26 colorectal tumor model compared to both free DEX and non-sensitive DEX conjugate. In addition, the effects of L–SS–DEX on TME modulation, including T cell infiltration, MDSCs, M1/M2 macrophages, as well as the expression of cyclooxygenase-2 (COX-2) and α-smooth muscle actin (α-SMA), were also evaluated in detail. As expected, L–SS–DEX showed great potential in relieve the immunosuppressive TME, resulting in superior therapeutic effect over free DEX. These results provide new possibilities for the application of anti-inflammatory drugs in cancer therapy.

2. Materials and methods

2.1. Materials

N-ε-benzyloxycarbonyl- L-lysine-*N*-carboxyanhydride (Lys(Z)-NCA) were synthesized based on our previous work [52]. 3-(4,5-Dimethylthiazol-2-yl)-2,5-diphenyl tetrazolium bromide (MTT), 3,3′-dithiodipropionic acid (DTPA), 4′,6-diamidino-2-phenylindole dihydrochloride (DAPI) and poly (ethylene glycol) monomethyl ether (mPEG, M_n = 5000) were bought from Sigma-Aldrich. Anhydrous *N'N*-dimetylformamide (DMF) was obtained through vacuum distillation. Dexamethasone (DEX) was bought from Dalian Meilun Biotechnology Co., LTD. Diisopropylcarbodiimide (DIC) was bought from Beijing J&K Co., LTD. Fluorescein isothiocyanate (FITC) was provided by Aladdin. Other reagents and solvents were provided by Sinopharm Chemical Reagent Co., LTD.

2.2. Characterization

^{1}H NMR spectra were characterized by Bruker AV-500 or Bruker AV-300 NMR spectrometer. Drug release and biodistribution experiments were calculated by high performance liquid chromatography (HPLC), which is made up of a Waters 2414 Refractive Index Detector, a Waters 515 HPLC pump and a reverse-phase C-18 column (Symmetry®). Dynamic light scattering (DLS) was used to characterize the sizes of the self-assemble nano-micelles. A JEOL JEM-1011 (Tokyo, Japan) was used to obtain transmission electron microscopy (TEM) images. Histological alterations were observed by optical microscope (Nikon Eclipse Ti, Optical Apparatus Co., Ardmore, PA, USA). All the immunofluorescence slides and cellular uptake slides were pictured through a confocal laser scanning microscope (CLSM, Carl Zeiss LSM 700, Germany).

2.3. Synthesis of polypeptide-DEX conjugates

Detailed synthesis method for mPEG-*b*-poly (L-lysine) (mPEG-*b*-PLL), 3,3′-Dithiodipropionic acid functionalized mPEG-*b*-PLL (mPEG-*b*-P (LL-DTPA)) and succinic acid functionalized mPEG-*b*-PLL (mPEG-*b*-P (LL-SA)) was described in the supplementary information, following our previously established method [36]. The polypeptide-DEX conjugates were prepared by esterification of hydroxyl in DEX with carboxyl on the side chains of mPEG-*b*-P (LL-DTPA) or mPEG-*b*-P (LL-SA). Take L–SS–DEX as an example. Briefly, mPEG-*b*-P (LL-DTPA) (800 mg, 0.09 mmol) was dispersed in anhydrous DMF. Then, the DMF solution of DEX (200 mg, 0.5 mmol), DMAP (36 mg, 0.3 mmol) and DIC (150 mg, 1.2 mmol) was injected into the above solution under stirring. After 36 h of continuous reaction, the mixture solution was poured into cold diethyl ether. The L–SS–DEX crude product was obtained and further purified through dialysis against deionized water for 72 h in dark and a flaxen solid was obtained after lyophilization.

2.4. Stimuli-responsive drug release

L–SS–DEX or L-SA-DEX (containing 0.5 mg DEX, dissolved in 5 mL buffer) was added to a dialysis bag (MW 3500 Da), and then immersed in 45 mL buffer under shaking (90 rpm) at 37 °C at three conditions: pH 7.4 (10 mM, phosphate buffered saline (PBS)), pH 7.4 with 10 mM glutathione (GSH) (10 mM, PBS), and pH 5.5 (10 mM, acetate buffer). At each time point, 5.0 mL of the release solution was withdrawn and 5.0 mL of the same fresh buffer was replenished. The release tests were repeated in triplicate under the same conditions. The amount of released DEX was measured by HPLC, with a mobile phase of water and acetonitrile (60/40, *V/V*) and a flow rate of 1.0 mL/min. The final release solution was also tested with high performance liquid chromatography-mass spectrometry (HPLC-MS), and the detailed experiment procedure is provided in the supporting information.

2.5. Cell lines and cell culture

The murine colorectal cancer CT26 cells were used to carry out the *in vitro* and *in vivo* studies. CT26 cells were culture with Dulbecco's modified Eagle's medium (DMEM) (containing 10% fetal bovine serum (FBS), 50 U/mL penicillin and 50 U/mL streptomycin) and incubated at

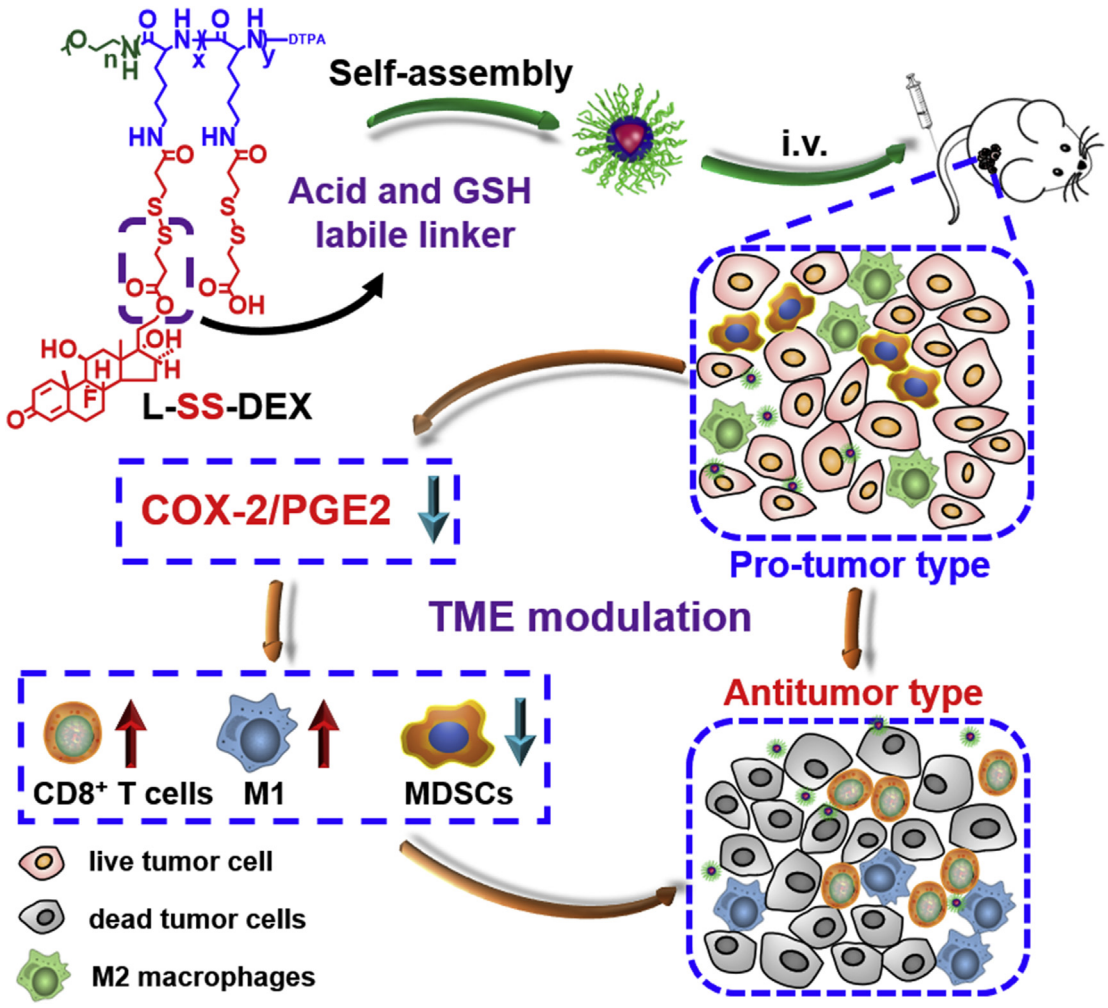

Scheme 1. Schematic illustration of L-SS-DEX for tumor microenvironment modulation. Intravenously injected L–SS–DEX selectively accumulates to the tumor by "EPR" effect, and release DEX in response to the low pH and redox microenvironment inside the tumor. Anti-inflammatory effects of DEX result in TME modulation, including increased $CD8^+$ T cells and M1 macrophages, decreased MDSCs, and significant tumor inhibition effect.

37 °C in an atmosphere of 5% CO_2.

2.6. In vitro cytotoxicity assays

The *in vitro* cytotoxicities of free DEX, L-SA-DEX and L–SS–DEX were evaluated using MTT assay. 8000 CT26 cells were seeded per well with 200 μL of complete culture medium to 96-well culture plates. After overnight incubation, free DEX and polypeptide-DEX (0–100 μg/mL DEX) was added. MTT assay test was carried out after incubation for another 24 or 48 h. The absorbances of each well were measured at 490 nm on a Bio-Rad 680 microplate reader. The relative cell viability (%) was determined through comparing the absorbance values of sample wells with that of control wells. The same method was used to evaluated the *in vitro* cytotoxicities of mPEG-*b*-P (LL-SA) and mPEG-*b*-P (LL-DTPA).

2.7. Cellular uptake

2×10^5 CT26 cells were seeded per well in a 6-well plate. After overnight incubation, the culture medium was replaced with fresh medium which contained FITC-labeled L-SA-DEX or L–SS–DEX micelles, respectively. After 1, 3 or 6 h incubation, the culture medium was removed, and the cultured cells were washed with cold PBS and fixed with PBS containing 4% (w/v) formaldehyde. Then the cell nuclei were stained with DAPI, and images were taken on a CLSM microscope.

2.8. Pharmacokinetics study

All animal studies were carried out according to the guidelines approved by the Animal Care and Use Committee of Jilin University. Female SD rats (average weight 220 g) were assigned into two groups at random ($n = 3$). DEX (10 mg/kg, dissolved in the 8:1:1 mixture of PBS and ethanol, Cremophor EL®) or L–SS–DEX (10 mg DEX/kg, dissolved in PBS) were administered via tail vein. Blood samples were collected from the orbital cavity through capillary tube at each desired time point (5 min, 0.5, 1, 2, 4, 8, 12 and 24 h), mixed with heparin sodium, and the plasmas were obtained after centrifugation, and was treated with 1 M hydrochloric acid following 1.2 M disodium hydrogen phosphate. Finally, the obtain plasmas were detected by HPLC according to the reported procedure [53]. The half-life of the drug ($t_{1/2}$) and area under the drug concentration–time curve from 0 to 24 h in plasma ($AUC_{0\text{-}t}$) were calculated using PKSolver [54].

2.9. Biodistribution study

The female BALB/c mice (6–8 weeks old) were subcutaneously embedded with CT26 cells (2×10^6) into the abdomen. Once the tumor volumes reached approximately 300 mm^3, free DEX or L–SS–DEX nanoparticles was intravenously injected into the mice at the same dose of DEX (10 mg/kg) ($n = 3$ per group). The tumor tissues and major organs (heart, liver, spleen, lung and kidney) were excised at predetermined

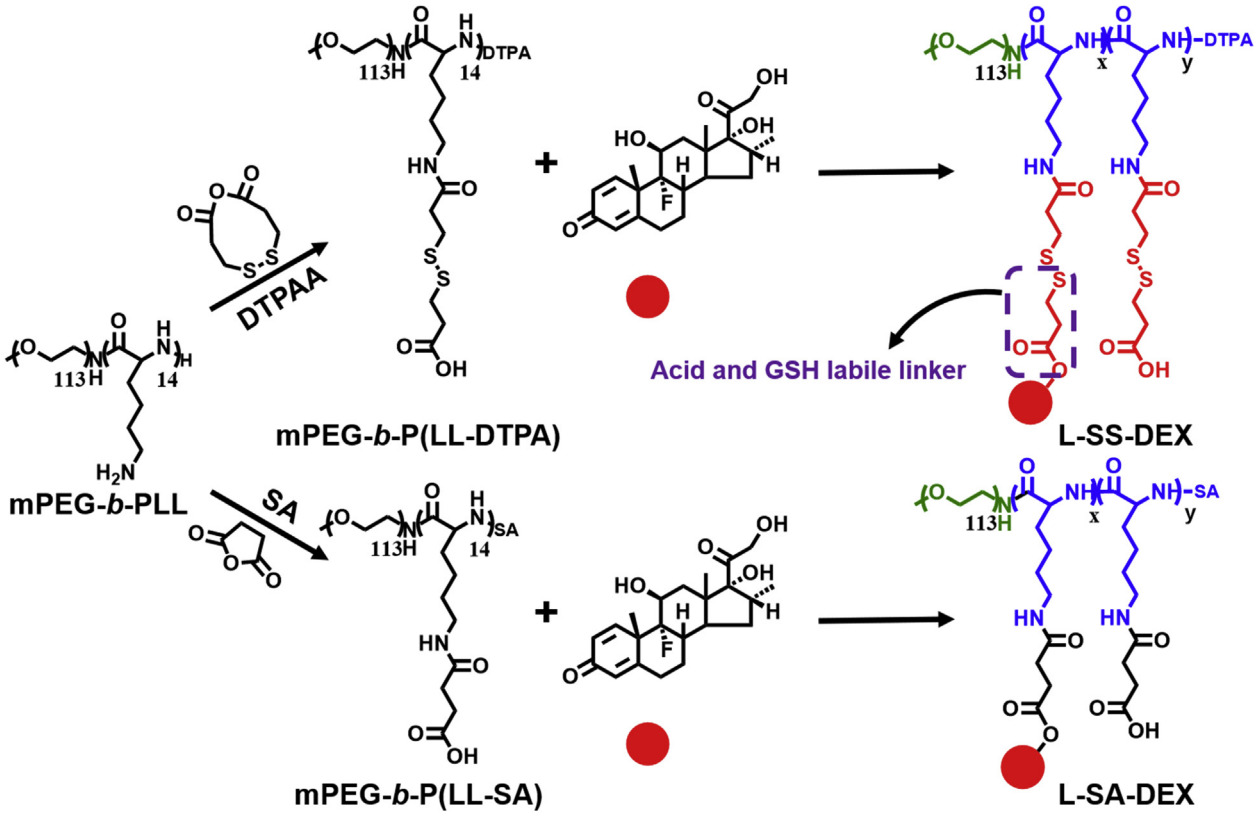

Fig. 1. Synthesis routes of L-SS-DEX and L-SA-DEX.

time points (6 h, 24 h, 48 h), accurately weighed and ground into pieces. The tissue debris was treated with 1 M hydrochloric acid following 1.2 M disodium hydrogen phosphate. Finally, the obtain supernatant was detected by HPLC according to the reported procedure [53].

2.10. In vivo antitumor efficiency

The female BALB/c mice (6–8 weeks old) were subcutaneously embedded with CT26 cells (2×10^6) into the abdomen. Once the tumor volume reached approximately 140 mm^3, the mice were assigned into 4 groups at random ($n = 5$) and received the treatment of PBS, DEX (10 mg/kg, dissolved in the 8:1:1 mixture of PBS and ethanol, Cremophor EL®), L-SA-DEX (10 mg/kg at DEX) or L–SS–DEX (10 mg/kg at DEX). The mice were intravenously injected with different formulations every three days and received six treatments in total. Body weights and tumor volumes were recorded every other day. The day when the treatment started was designated as day 0. The tumor volume was measured with calipers and calculated as following: tumor volume (V) = $a \times b^2/2$, where a is the major axis and b is the minor axis of the tumor. The tumor suppression rate (TSR) was calculated as following: TSR (%) = $[(V_c - V_x)/V_c] \times 100\%$, where V_c represents the mean tumor volume of the PBS group and V_x represents the mean tumor volume of the treatment group.

2.11. Immunohistochemical and immunofluorescence analyses

Mice were sacrificed on day 16, major organs and tumors were obtained, and soaked into 4% PBS buffered paraformaldehyde for 24 h, then soaked into 15% (w/v) and 30% (w/v) PBS-buffered sucrose solution successively, and finally all the organs and tumor tissues were kept in 30% (w/v) PBS-buffered sucrose solution before use. To obtain paraffin slices, the paraffin embedded tissues were cut into 5 μm thickness. Histological alterations of tumors and the major organs were evaluated by staining the paraffin slices with hematoxylin and eosin (H &E). Immunofluorescence analyses was carried out on frozen sections using antibodies against COX-2, α-SMA, CD3, CD4 and CD8. TUNEL staining was carried out following the manufacturer's protocol (KeyGen Biotech, KGA703).

2.12. Flow cytometry analysis

To analyze the immune cells in the tumor tissues, the harvested tumors were digested using tumor dissociation buffer. Single-cell suspensions were obtained after nylon mesh filtration, and incubated with various antibodies against the immune cells (Table S2), following a previously published procedure [55]. FACS test was carried out on a flow cytometry machine (BECKMAN COULTER, CytoFLEX). The results were analyzed with the CytExpert (BECKMAN COULTER).

2.13. Inflammatory cytokines analyses

To analyze inflammatory cytokines in the tumor tissues, the harvested tumors were homogenized in PBS buffer, and the supernatant was obtained after centrifugation. Cytokines in the supernatant, including interferon-gamma (IFN-γ), tumor necrosis factor alpha (TNF-α), interleukin 4 (IL-4), interleukin 10 (IL-10) and prostaglandin E2 (PGE2), were detected using ELISA kits (Table S3). All the tests were carried out following the manufacturer's protocols.

2.14. Statistical analyses

All experiments were performed at least three times and expressed as means ± standard deviation (SD). For comparison between two groups, student's *t*-test was used. For comparison between multiple groups, one-way ANOVA was used.

3. Results and discussion

3.1. Synthesis and characterization of polypeptide–DEX conjugates

The synthesis method of mPEG-*b*-P (LL-DTPA) and mPEG-*b*-P (LL-SA) is consistent with our previous work [36]. As high glutathione concentration is a basic hallmark of cancer cells [42], 3,3′-dithiodipropionic acid was used to modify the side chain to introduce disulfide linker between drug and the carriers, while the succinic acid modified mPEG-*b*-PLL (mPEG-*b*-P (LL-SA)) was synthesized as a control. All the peaks of the resulting copolymers, mPEG-*b*-P (ZLL), mPEG-*b*-PLL, mPEG-*b*-P (LL-DTPA) and mPEG-*b*-P (LL-SA), were well assigned in the ^{1}H NMR spectra (Fig. S1). DEX was conjugated to the two kinds of polypeptides by esterification of hydroxyl in DEX with carboxyl on the side chains of polypeptides, and resulted in L–SS–DEX and L-SA-DEX (Fig. 1). There are three hydroxyl groups in DEX, while the one at beta position of the carbonyl is more reactive due to less steric hindrance. In L–SS–DEX, the chemical shifts of methylene at the carbonyl beta position (*j*) in DEX switched from δ 4.53–4.45 (dd, 1H) ppm and δ 4.04–4.02 (d, 1H) ppm to δ 5.08 (d, 1H) ppm and δ 4.83–4.80 (d, 1H) ppm, and the hydrogen peak in the reactive hydroxyl disappeared, which should be at δ 4.7 ppm (*r*) in the free DEX in ^{1}H NMR spectrum (Fig. 2A and B). By comparing the characteristic peaks intensities of DEX at δ 7.30 (d, 1H) ppm, δ 6.22 (dd, 1H) ppm and δ 6.01 (s, 1H) ppm with the proton intensities of mPEG at δ 3.8 ppm, the average conjugate number of DEX was about 5.0 per polypeptide, and the drug loading content was 17.1 wt%. L-SA-DEX was also successfully synthesized as confirmed by ^{1}H NMR spectrum (Fig. S2). The average conjugate number of DEX was about 3.2 per polymer, and the drug loading content was 13.2 wt%.

3.2. Self-assembly and in vitro drug release of polypeptide-DEX conjugates

Due to the amphiphilicity, both L-SA-DEX and L–SS–DEX can easily dissolve in PBS and assemble into micelles. The hydrodynamic radii (R_h) of L-SA-DEX and L–SS–DEX micelles determined by DLS were about 38 and 33 nm, respectively (Fig. S3A). The sizes of L-SA-DEX and L–SS–DEX micelles will conduce to better accumulation in tumor tissues via EPR effect [56]. The zeta potentials of L-SA-DEX and L–SS–DEX micelles were about −7.8 mV and −5.2 mV, respectively. To evaluate the stability of the micelles, the sizes of L-SA-DEX and L–SS–DEX micelles in PBS medium with 10% FBS were monitored by DLS for 72 h. The sizes of the two self-assembled micelles did not change much during the observation period, suggesting the prepared micelles could keep stable once getting contact with plasma. This may be due to the existence of PEG, which contributed to reduce the adsorption of protein, and the hydrophobic moiety ensured that micelles formed a stable core (Fig. S3B). TEM images further confirmed the uniform size and spherical morphologies of L-SA-DEX and L–SS–DEX, the average diameters of L-SA-DEX and L–SS–DEX micelles measured by TEM were around 32 and 29 nm, respectively (Figs. S3C and D).

Tumor tissue is infiltrated with a large number of pro-inflammatory cytokines and immunosuppressive cells [55,57]. Therefore, sustained and effective release of drug is of great significance for the regulation of tumor microenvironment [40]. Polymer-drug conjugates can efficiently increase the accumulation and protracted retention at the tumor tissue

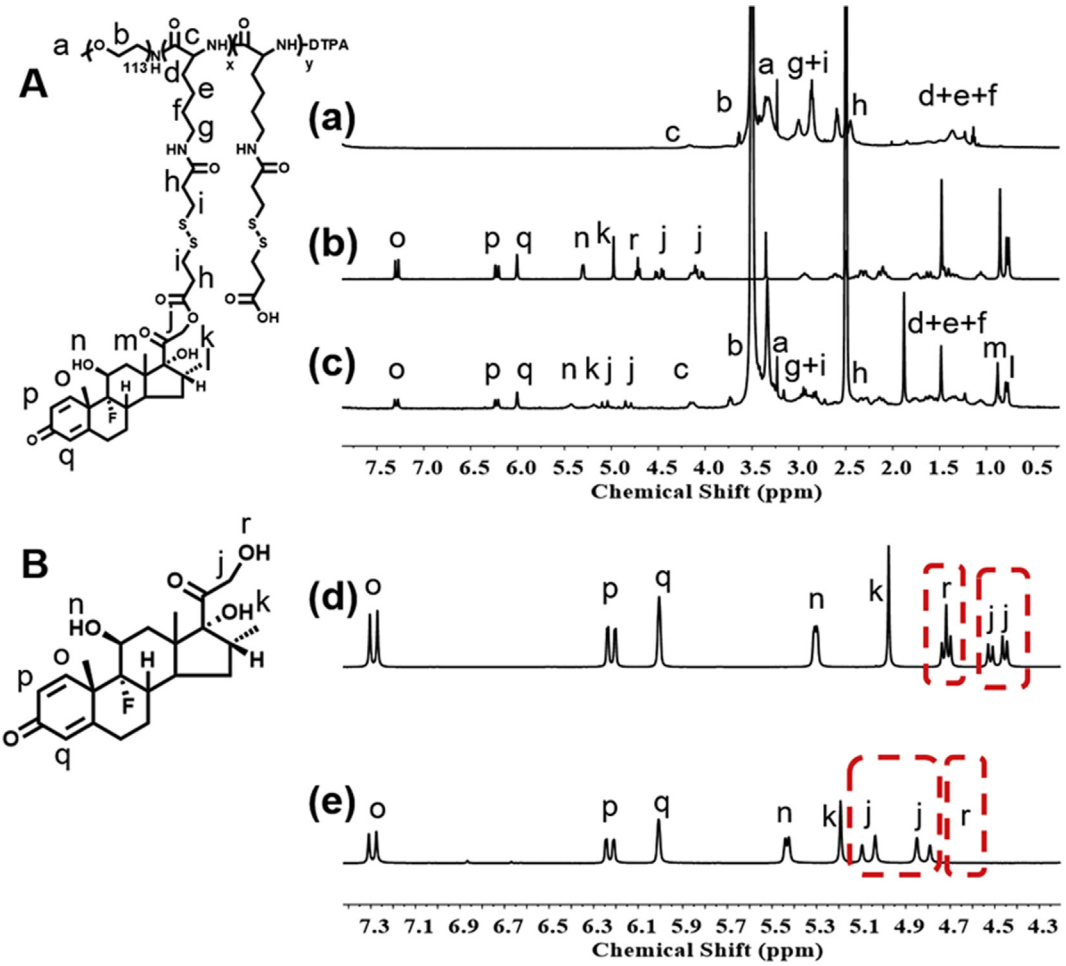

Fig. 2. ^{1}H NMR spectrum of L-SS-DEX. (A) ^{1}H NMR spectra of mPEG-*b*-P (LL-DTPA) (a), DEX (b) and L–SS–DEX (c) in DMSO-d_6. (B) The characteristic chemical shifts changes of DEX in L–SS–DEX conjugates (e) compared with free DEX (d).

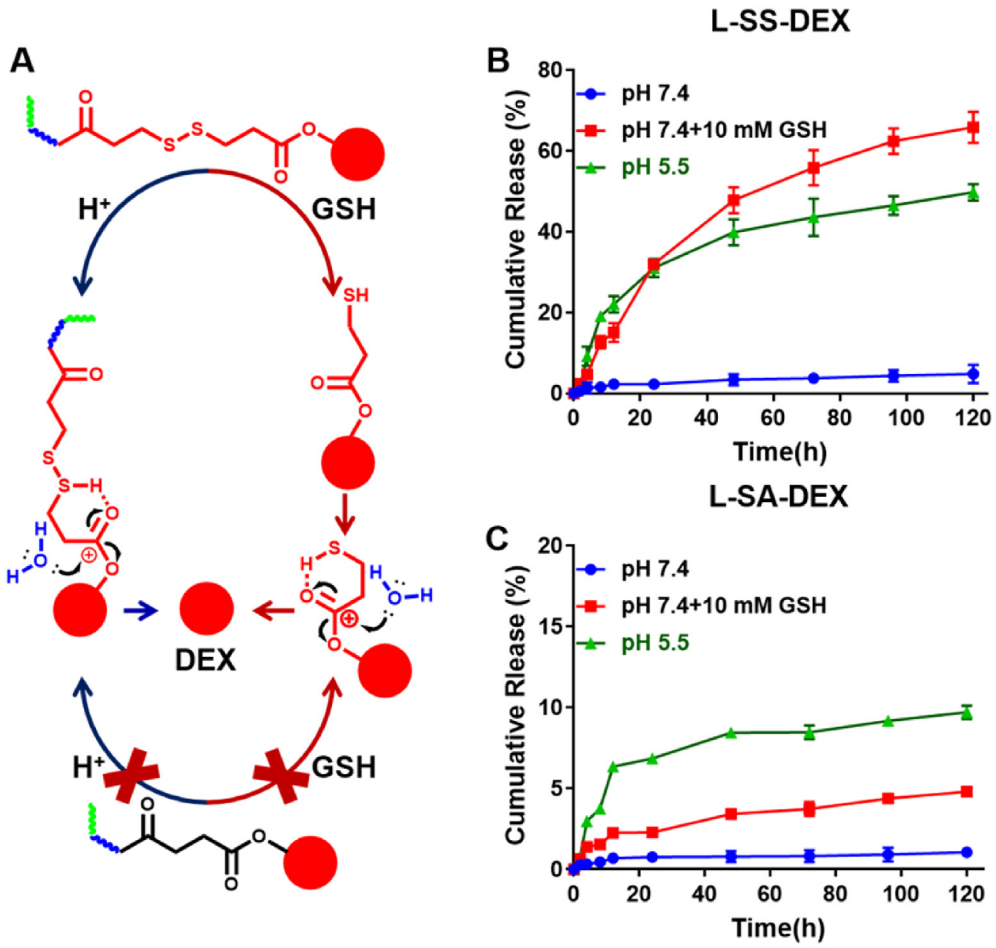

Fig. 3. Release study of polypeptides-DEX. (A) Schematic illustrations of hypothetical release mechanism of DEX from L–SS–DEX and L-SA-DEX. (B–C) *In vitro* DEX release profiles of L–SS–DEX and L-SA-DEX in buffer containing 0.2% (w/v) Tween 80 at various simulated conditions: pH 7.4, pH 7.4 with 10 mM GSH and pH 5.5. The release experiments were repeated in triplicate under the same conditions. Data were presented as the mean ± SD (n = 3).

by EPR effect, which prolongs the acting time of drugs [58]. Tumor endosome (pH ≈ 5–6) is significantly acidic than the normal tissues (pH ≈ 7.4) [59], which will increase the protonation degree of β-thiopropionate, and subsequently active the neighbouring ester bonds (Fig. 3A). The release rate of DEX was faster in the condition of pH 5.0 compared with that of pH 7.4, and 49% of the total amount of DEX released from L–SS–DEX micelles at the end (120 h). All these proved that L–SS–DEX had the ability of enhanced acid-triggered release. The disulfide bonds can be cut off in the presence of GSH, and the exposed thiol groups are linked with the carbonyl group to release the drug. There was more than 66% of DEX released from L–SS–DEX micelles at pH 7.4 with 10 mM GSH as the trigger. All these results proved the pH and GSH dual-responsiveness of DEX release from L–SS–DEX (Fig. 3B). The release of DEX from L-SA-DEX micelles was slow and insensitive to acidic and GSH. There was only less than 10% of DEX released from the L-SA-DEX in 120 h (Fig. 3C). We further used HPLC-MS to detect the release solution obtained at the final time point of the release experiment. As shown in Fig. S4, the released DEX matched the parent compound in the presence of GSH or in the condition of pH 5.5, and the accumulative release rate determined by HPLC-MS was in consistent with that obtained from HPLC with a UV detector (Table S1).

3.3. *In vitro* cytotoxicities and cellular uptake

The cytotoxicity of mPEG-*b*-P (LL-DTPA) and mPEG-*b*-P (LL-SA) were carried out on CT26 murine colon tumor cells by MTT assays. After incubation for 24 h or 48 h, no obvious cytotoxicity was observed in both materials even at 1000 μg/mL (Fig. 4A). Similar to free DEX, both L–SS–DEX and L-SA-DEX didn't show obvious cytotoxicity to CT26 cells (Fig. 4B).

Internalization of L–SS–DEX and L-SA-DEX micelles was evaluated with CLSM using FITC labeled L–SS–DEX and L-SA-DEX. As shown in Fig. 4C, green fluorescence of FITC could be observed and uniformly distributed in the cell cytoplasm after incubation for 3 h. When the incubation time was extended to 6 h, much stronger green fluorescence ascribing to FITC moieties could be observed in L-SA-DEX or L–SS–DEX treated cells. All these results proved that L-SA-DEX and L–SS–DEX could be endocytosed by tumor cells.

3.4. *Pharmacokinetics*

The pharmacokinetics of L–SS–DEX and free DEX were investigated in SD rats. As shown in Fig. 5, L–SS–DEX micelles could extend the blood circulation time ($t_{1/2}$ = 8.93 ± 0.65 h) compared with free DEX ($t_{1/2}$ = 3.54 ± 0.35 h). Free DEX was quickly cleared from blood circulation and couldn't be detected at 12 h post injection. As shown in Table 1, the $AUC_{0\text{-}t}$ of the L–SS–DEX in 24 h was 95.72 ± 10.30 μg/mL h, which was much higher than that of the free DEX (8.78 ± 2.07 μg/mL h). All these results demonstrated L–SS–DEX possessed longer half-life and superior bioavailability compared with free DEX.

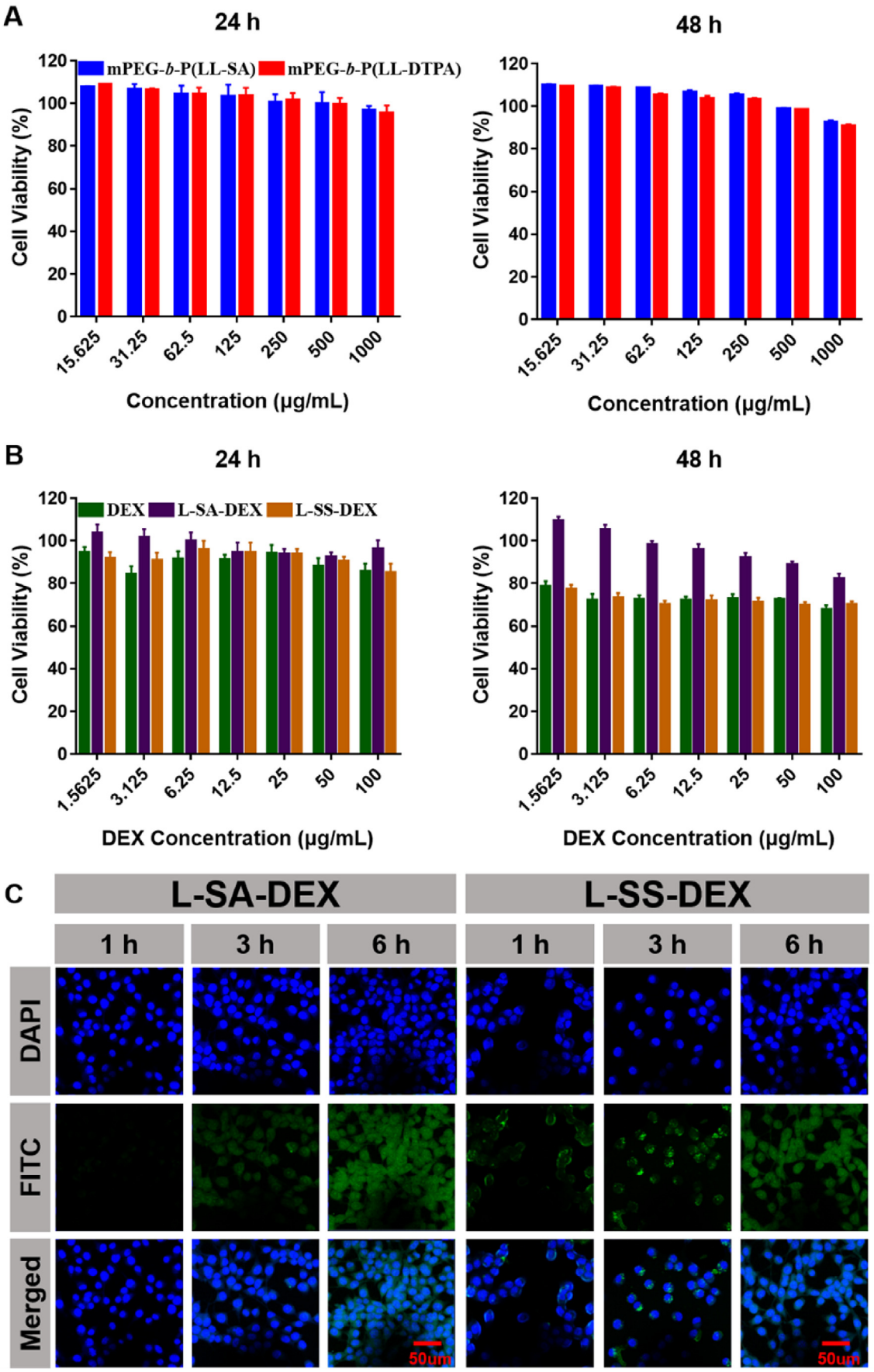

(caption on next page)

Fig. 4. *In vitro* cytotoxicity and cellular uptake study. (A) *In vitro* cytotoxicities of mPEG-*b*-P (LL-SA) and mPEG-*b*-P (LL-DTPA) to CT26 cells at different polymer concentrations after incubation for 24 and 48 h (n = 5). (B) *In vitro* cytotoxicities of free DEX, L-SA-DEX and L–SS–DEX to CT26 cells at different DEX concentrations after incubation for 24 and 48 h (n = 5). Data were presented as the mean ± SD. (C) CLSM images of cellular uptake by CT26 cells after incubation with FITC-labeled L-SA-DEX and FITC-labeled L–SS–DEX for 1, 3 and 6 h.

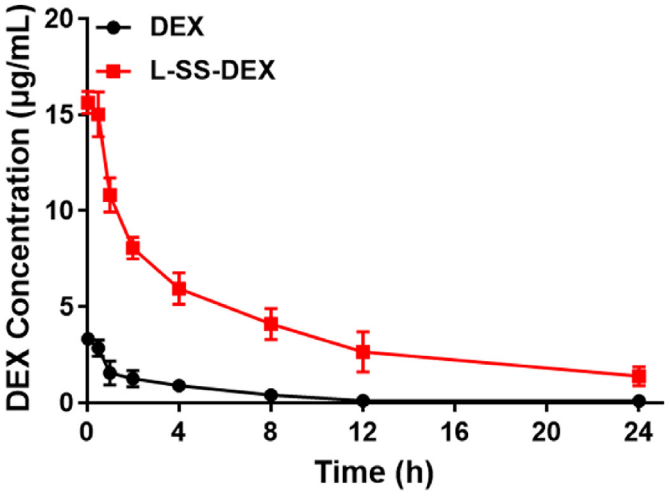

Fig. 5. Pharmacokinetic results of free DEX and L-SS-DEX in SD rats. All DEX formulations were administered at equivalent DEX dose of 10 mg/kg. Data were shown as means ± SD (n = 3).

Table 1
Pharmacokinetic parameters estimated for free DEX and L-SS-DEX in SD rats.

	$t_{1/2}$[a] (h)	AUC_{0-t}[b] (μg/mL h)
DEX	3.54 ± 0.35	8.78 ± 2.07
L–SS–DEX	8.93 ± 0.65	95.72 ± 10.30

[a] $t_{1/2}$: half-life.
[b] AUC_{0-t}: area under the drug concentration–time curve from 0 to 24 h in plasma.

3.5. Biodistribution

The biodistribution of L–SS–DEX compared to free DEX was assessed in CT26 tumor bearing mice. After one intravenous injection, the accumulation of DEX in tumors of the L–SS–DEX group was much higher than that of the free DEX group, which was about 4.4 folds (at 6 h), 8.2 folds (at 24 h) and 9.7 folds (at 48 h), respectively (Fig. 6). This result demonstrated that L–SS–DEX had better tumor accumulation ability than free DEX. The accumulation of L–SS–DEX in major organs was higher than free DEX, which might be attributed to the prolonged circulation time of L–SS–DEX. But the concentration of L–SS–DEX in major organs tended to decrease over time, which meant that L–SS–DEX could be removed from these organs including liver and kidney. At 48 h after injection, the cumulative ratio of L–SS–DEX in tumor to kidney, liver and lung was 1.7, 1.03 and 5.16, respectively, which was much higher than that of free DEX (0.27, 0.26 and 0.91) (Table S4), indicating the accumulation of DEX in solid tumors was significantly enhanced in the L–SS–DEX formulation compared to the free form.

3.6. Hematological analysis

Before *in vivo* therapeutic study, we firstly carried out the routine blood tests and blood chemistry analysis to evaluate the tolerability and toxicities of the DEX in various formulations for BALB/c mice. Healthy BALB/c mice received 6 times different treatments, and whole blood cells and serum was analyzed at 24 h after the last treatment. As shown in Fig. S6, there were no significant difference in hematological parameters between the L–SS–DEX treated group and PBS group, including

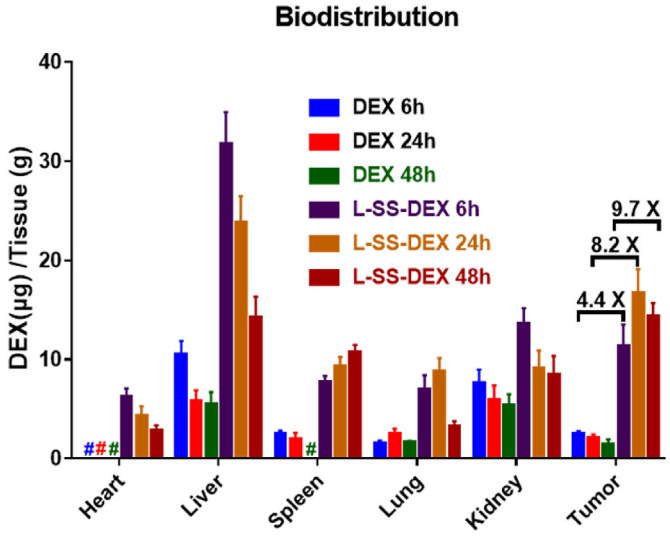

Fig. 6. Biodistribution results of free DEX and L-SS-DEX in CT26 tumor-bearing mice. All DEX formulations were administered at equivalent DEX dose of 10 mg/kg. Data were shown as means ± SD (n = 3). # indicated the value was below the detection limit by HPLC.

white blood cell (WBC), red blood cells (RBC), hemoglobin (HGB) and hematocrit (HCT), while free DEX significantly reduced the white blood cell numbers. All treatments did not cause significant alterations in alanine transaminase (ALT), aspartate aminotransferase (AST) and creatinine (CREA), which meant no obvious influence in liver and kidney functions (Fig. S7). The above results prove that L–SS–DEX has better tolerability than free DEX in BALB/c mice.

3.7. In vivo antitumor efficacy

Murine colon cancer CT26 cells model was chosen for *in vivo* antitumor study. When the tumors reached about 140 mm^3, mice received the treatment of PBS, free DEX, L-SA-DEX or L–SS–DEX every three days for a total of six times on day 0, 3, 6, 9, 12 and 15. The injected DEX doses were all 10 mg/kg on DEX basis (Fig. 7A). As shown in Fig. 7B, tumors in the PBS group grew fast, and the tumor volume reached approximately 2000 mm^3 on day 16. The treatment of free DEX did not show too much ability in tumor inhibitions as the average tumor volume reached about 900 mm^3 by the end of the observation (TSR % = 49%). The treatment of L-SA-DEX showed modest therapeutic effect (TSR% = 41%), which might be imputed to the low efficient DEX release from L-SA-DEX. However, the L–SS–DEX showed the permanent tumor inhibition effect during the whole treatment compared to other groups, and resulted in a TSR% of 86% on day 16. More importantly, there is no significant body weight loss during the treatments (Fig. 7C). L–SS–DEX treatment significantly prolonged the median survival time of mice, which was about 1.6 times to PBS and 1.4 times to free DEX or L-SA-DEX (Fig. 7D).

3.8. Histological and immunofluorescence analysis

Histological analysis and immunofluorescence staining were performed to further evaluate the antitumor activity, the modulation of tumor microenvironment and the safety of the treatments. Large areas of necrosis (especially in the central part of the tumor) were observed in the L–SS–DEX treated group, as compared to the other groups (Fig. 8A).

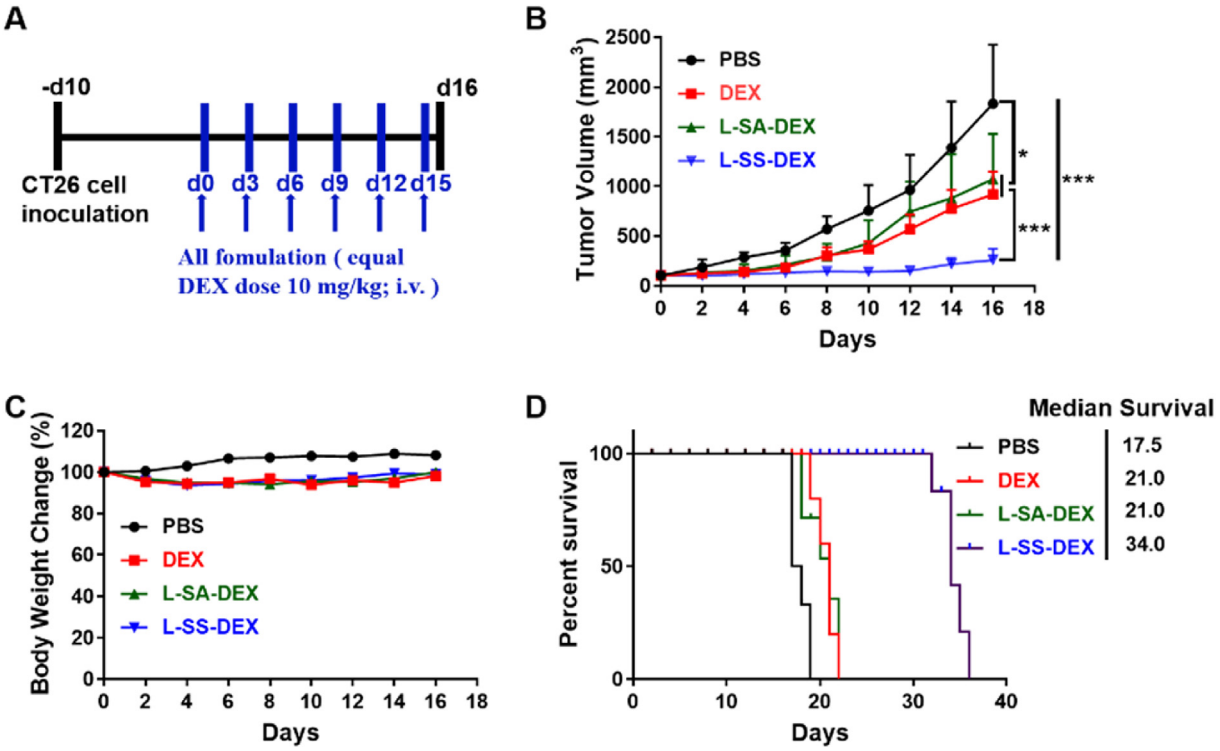

Fig. 7. Therapeutic results in CT26 tumor model. (A) The therapeutic schedule of the *in vivo* study. (B–D) Tumor volume, body weight changes and survival curves of CT26 tumor-bearing mice after receiving various treatments; $n = 5$. Results are presented as means ± SD; *p < 0.05, ***p < 0.001.

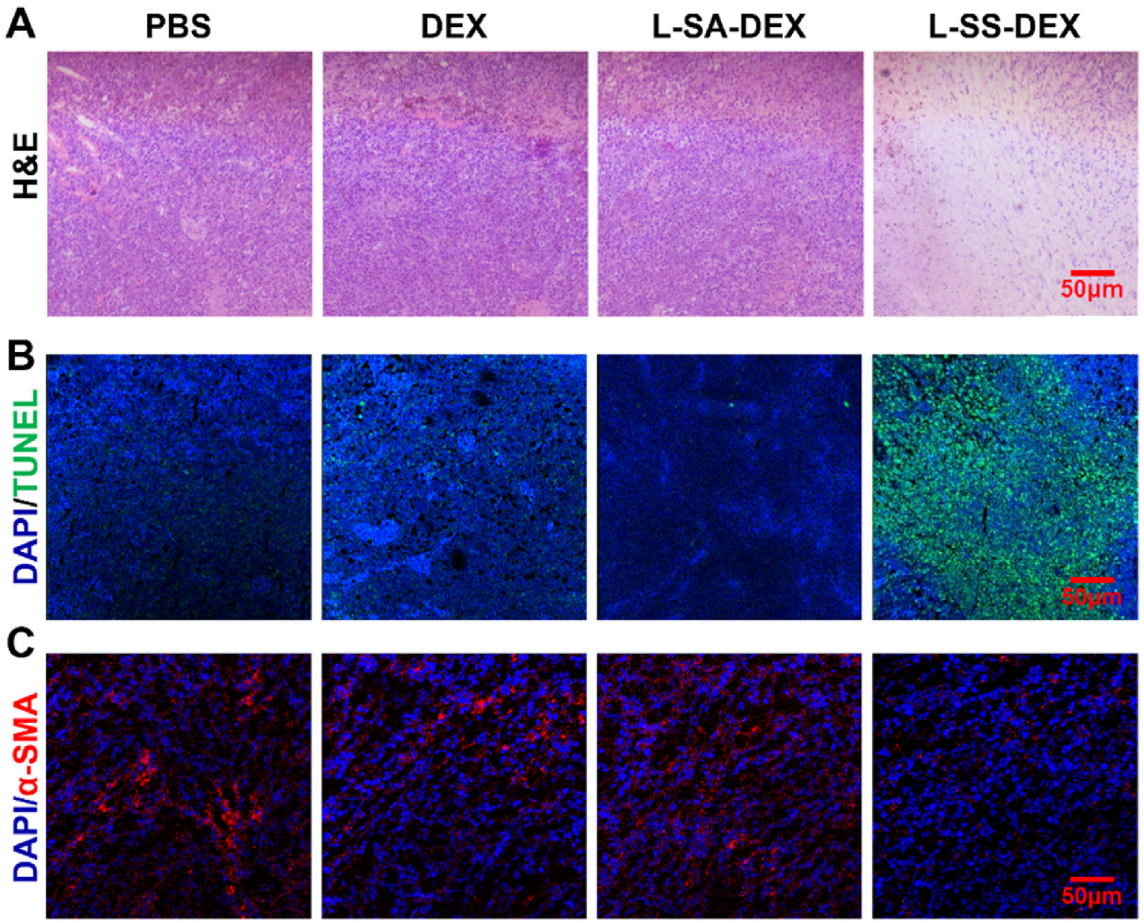

Fig. 8. Histological and immunofluorescence staining of the tumors after various treatments. (A) H&E staining, (B) TUNEL staining and (C) α-SMA staining of tumor sections after different treatments.

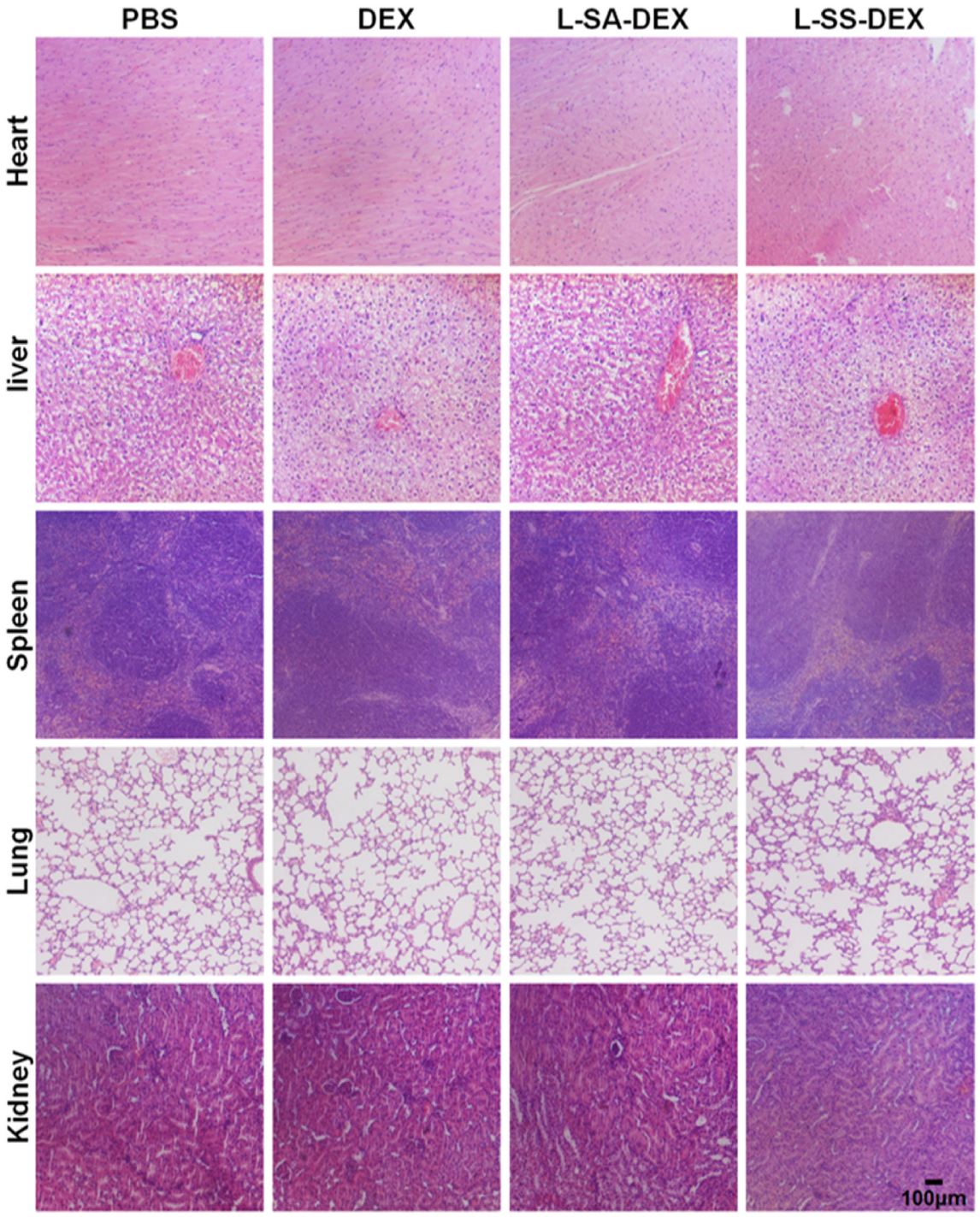

Fig. 9. Histological analysis of different organs (heart, liver, spleen, lung and kidney) after various treatments.

TUNEL assay was also introduced to evaluate the apoptosis in the tumor. Consistent with H&E results, much stronger green fluorescence was observed in the tumors of the L–SS–DEX treated group, which revealed higher cell necrotic and apoptosis after the treatment of L–SS–DEX (Fig. 8B and Fig. S8). Besides, the treatment of L–SS–DEX also significantly reduced the content of α-SMA at the tumor proliferating margin areas (Fig. 8C and Fig. S9). α-SMA is a symbol of activated tumor-associated fibroblasts. Decreased fibrosis in tumor tissues will increase the permeability of tumors, which may be helpful for the infiltration of nanoparticles as well as cytotoxic T lymphocytes. The major organs (heart, liver, spleen, lung and kidney) were also stained by H&E to evaluate the safety of these treatments. The major organs of all the treatment groups showed normal histomorphology and no pathological abnormality was observed, suggesting no obvious systemic toxicity of the treatments (Fig. 9).

3.9. Tumor immune microenvironment evaluation

COX-2, an inflammatory stress kinase which catalyzes the formation of PGE2 [60], gives free rein to tumor immune evasion and resistance to cancer immunotherapy. DEX has been proved to exert its anti-inflammatory effects through destabilizing the COX-2 mRNA by inhibiting the mitogen-activated protein kinase p38 [61]. Thus, we further analyzed the COX-2 expression inside the tumor tissues by

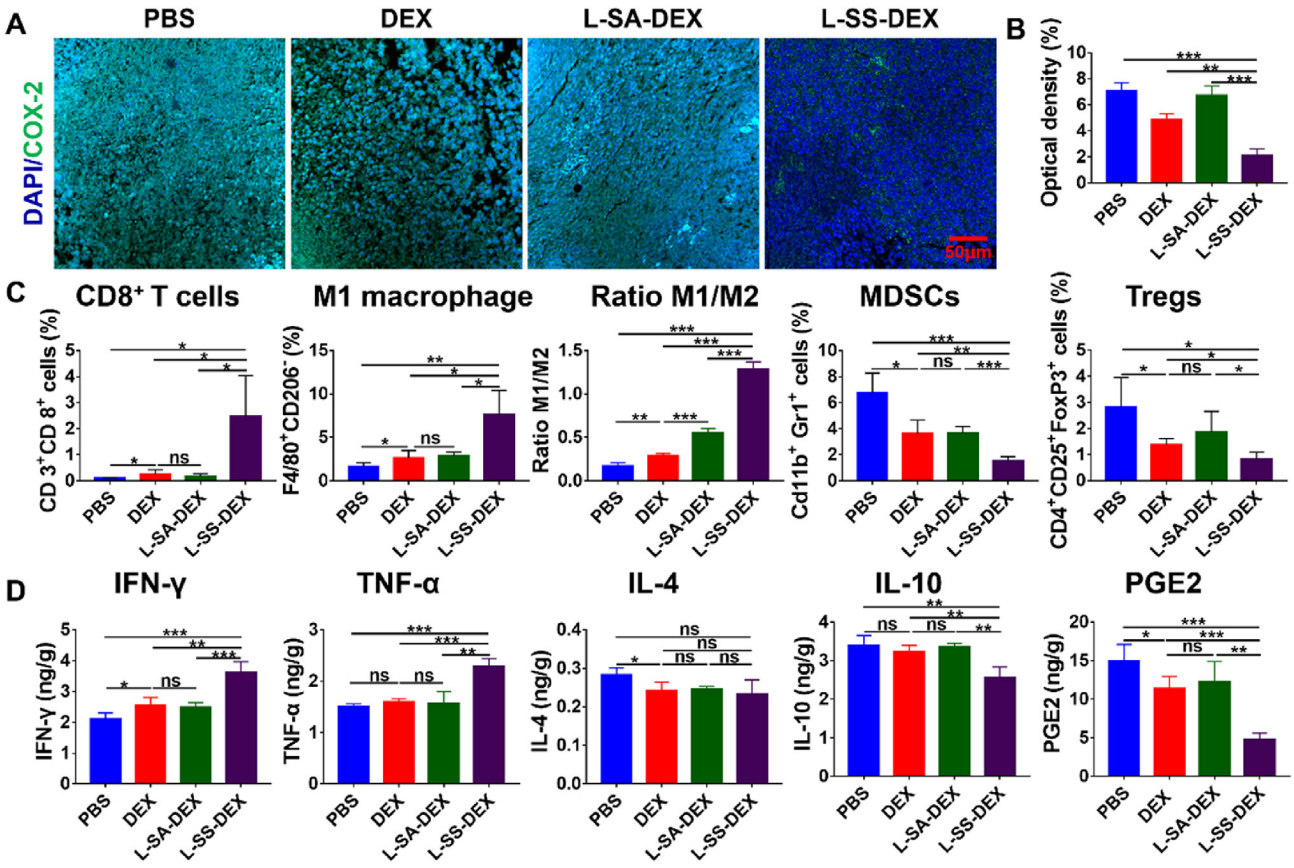

Fig. 10. Tumor immune microenvironment evaluation after various treatments. (A) COX-2 immunofluorescence staining of CT26 tumor tissues, COX-2 (green), DAPI (blue). (B) Relative optical densities of tumor sections from COX-2 staining; $n = 3$. (C) Flow cytometry analysis immune cells in TME after different treatments; $n = 4$. (D) The content of various cytokines in tumors: IFN-γ, TNF-α, IL-4, IL-10 and PGE2; $n = 4$. Results are presented as means ± SD; *p < 0.05, **p < 0.01, ***p < 0.001; ns, no significance. (For interpretation of the references to color in this figure legend, the reader is referred to the Web version of this article.)

immunofluorescence staining and Western blot analysis. As shown in Fig. 10A and B and Fig. S10, the expression of COX-2 was significantly reduced in L–SS–DEX treated group compared with PBS treated group and other DEX formations treated groups. Western blot quantitative analysis also confirmed this trend (Fig. S11). The reduction in COX-2 expression should benefit for relieve the immunosuppressive tumor microenvironment. To confirm this, we tested the immune cell populations inside the tumor after various treatments by flow cytometry analysis and immunofluorescence. As shown in Fig. 10B, L–SS–DEX treatment resulted in an increase in $CD8^+$ T cells inside the tumor, as well as increase in M1 type macrophages and M1/M2 ratios, while Tregs and MDSCs were much decreased (Fig. S12 and Fig. S13). The increase of M1/M2 macrophages means that the tumor is changing from a tumor-promoting inflammation status into a tumor-suppressing inflammation status. Free DEX and L-SA-DEX showed weak effect on these changes. Immunofluorescence staining confirmed these changes. Specially, there are no significant changes in $CD4^+$ T cells (Fig. S14), while the $CD8^+$ T cells were increased (Fig. S15).

We further analyzed the expression of various cytokines inside the TME after various treatments. As shown in Fig. 10D, the expression of the Th1 type cytokines IFN-γ and TNF-α were both enhanced in L–SS–DEX treated group compared to other groups, which is consistent with the increase of $CD8^+$ cells and M1 macrophages. Although there was no significant difference in the expression of IL-4 in all groups, a reduction of Th2 type cytokine IL-10 was observed after the treatment of L–SS–DEX, while other treatments had no such effects. As the content of COX-2 decreased, the secretion of PGE2 was also much reduced after L–SS–DEX treatment. PGE2 is an important regulatory cytokine secreted by tumor cells in maintaining the immunosuppressive tumor microenvironment. The decrease in PGE2 explained the changes of MDSCs and Tregs ratios inside the tumor after L–SS–DEX treatments.

4. Conclusion

In this study, we developed a polypeptide–DEX conjugate for neutralizing tumor-promoting inflammation for colorectal cancer therapy. This conjugate showed pH and redox dual sensitive release of DEX, and much enhanced accumulation of DEX inside the tumor tissue (9.7-fold over free DEX after 48 h). *In vivo* anti-tumor studies showed that the polypeptide-DEX conjugates markedly inhibited murine CT26 tumor growth as compared to free DEX or insensitive conjugates. Besides, the polypeptide-DEX conjugates significantly increased the $CD8^+$ T cell infiltration and the M1 over M2 macrophages ratios while decreased the content of immunosuppressive MDSCs and Tregs inside the tumor. Further analysis revealed that the inhibition in COX-2 and PGE2 may be the major reasons of L–SS–DEX in reversal the immunosuppressive microenvironment of the tumor.

We have to mention that the therapeutic effect of neutralizing tumor-promoting chronic inflammation may be tumor type-dependent. In most occasions, cancer occurs at sites of chronic inflammation, and the abundant immune cells maintain an immunosuppressive microenvironment and stimulate tumor cell proliferation. Therefore, applying anti-inflammation therapy should be helpful in reversal of the immunosuppressive TME and in tumor growth inhibition. In some other occasions like sarcomas, there lacks enough immune cell infiltration, and strategies to increase immune cell infiltration to stimulate these “cold” tumor into “hot” are necessary. Since epithelial cell cancers are mainly accompanied with chronic inflammation, we believe our study

suggested a promising approach in using properly designed anti-inflammatory drug formulations for cancer therapy.

Declaration of competing interest

The authors declare no conflict of interests.

Acknowledgement

This work is supported by the National Natural Science Foundation of China (51673185, 51673189, 51833010, 51520105004, and 51973215), the Jilin Province Science and Technology Development Plan (20170101100JC, 20190103112JH), and Ministry of Science and Technology of China (2016YFC1100701).

Appendix A. Supplementary data

Supplementary data to this article can be found online at https://doi.org/10.1016/j.biomaterials.2019.119676.

References

[1] L.M. Coussens, Z. Werb, Inflammation and cancer, Nature 420 (2002) 860–867.
[2] L.M. Coussens, L. Zitvogel, A.K. Palucka, Neutralizing tumor-promoting chronic inflammation: a magic bullet? Science 339 (2013) 286–291.
[3] S.I. Grivennikov, F.R. Greten, M. Karin, Immunity, inflammation, and cancer, Cell 140 (2010) 883–899.
[4] W. Song, K. Tiruthani, Y. Wang, L. Shen, M. Hu, O. Dorosheva, et al., Trapping of lipopolysaccharide to promote immunotherapy against colorectal cancer and attenuate liver metastasis, Adv. Mater. 30 (2018) e1805007.
[5] Y. Chen, W. Song, L. Shen, N. Qiu, M. Hu, Y. Liu, et al., Vasodilator hydralazine promotes nanoparticle penetration in advanced desmoplastic tumors, ACS Nano 13 (2019) 1751–1763.
[6] B.Z. Qian, J.W. Pollard, Macrophage diversity enhances tumor progression and metastasis, Cell 141 (2010) 39–51.
[7] R. Kim, M. Emi, K. Tanabe, K. Arihiro, Tumor-driven evolution of immunosuppressive networks during malignant progression, Cancer Res. 66 (2006) 5527–5536.
[8] K.E. de Visser, A. Eichten, L.M. Coussens, Paradoxical roles of the immune system during cancer development, Nat. Rev. Cancer 6 (2006) 24–37.
[9] H. Kim, H. Chung, J. Kim, D.-H. Choi, Y. Shin, Y.G. Kang, et al., Macrophages-triggered sequential remodeling of endothelium-interstitial matrix to form pre-metastatic niche in microfluidic tumor microenvironment, Adv. Sci. 6 (2019).
[10] A. Mantovani, M. Muzio, C. Garlanda, S. Sozzani, P. Allavena, Macrophage Control of Inflammation: Negative Pathways of Regulation of Inflammatory Cytokines, (2001).
[11] J. Condeelis, J.W. Pollard, Macrophages: obligate partners for tumor cell migration, invasion, and metastasis, Cell 124 (2006) 263–266.
[12] J. Cuzick, F. Otto, J.A. Baron, P.H. Brown, J. Burn, P. Greenwald, et al., Aspirin and non-steroidal anti-inflammatory drugs for cancer prevention: an international consensus statement, Lancet Oncol. 10 (2009) 501–507.
[13] Z.-D. Shi, X.-M. Qian, C.-Y. Liu, L. Han, K.-L. Zhang, L.-Y. Chen, et al., Aspirin-/TMZ-coloaded microspheres exert synergistic antiglioma efficacy via inhibition of beta-catenin transactivation, CNS Neurosci. Ther. 19 (2013) 98–108.
[14] S. Khan, S. Setua, S. Kumari, N. Dan, A. Massey, B. Bin Hafeez, et al., Superparamagnetic iron oxide nanoparticles of curcumin enhance gemcitabine therapeutic response in pancreatic cancer, Biomaterials 208 (2019) 83–97.
[15] Y. Zhang, L. Liu, P. Fan, N. Bauer, J. Gladkich, E. Ryschich, et al., Aspirin counteracts cancer stem cell features, desmoplasia and gemcitabine resistance in pancreatic cancer, Oncotarget 6 (2015) 9999–10015.
[16] X.W. Hua, A.I. Phipps, A.N. Burnett-Hartman, S.V. Adams, S. Hardikar, S.A. Cohen, et al., Timing of aspirin and other nonsteroidal anti-inflammatory drug use among patients with colorectal cancer in relation to tumor markers and survival, J. Clin. Oncol. 35 (2017) 2806.
[17] A.C. Vidal, L.E. Howard, D.M. Moreira, R. Castro-Santamaria, G.L. Andriole, S.J. Freedland, Aspirin, NSAIDs, and risk of prostate cancer: results from the REDUCE study, Clin. Cancer Res. 21 (2015) 756–762.
[18] D. Kumar, H. Rahman, E. Tyagi, T. Liu, C. Li, R. Lu, et al., Aspirin suppresses PGE(2) and activates AMP kinase to inhibit melanoma cell motility, pigmentation, and selective tumor growth in vivo, Cancer Prev. Res. 11 (2018) 629–641.
[19] C.E. Holmes, J. Jasielec, J.E. Levis, J. Skelly, H.B. Muss, Initiation of aspirin therapy modulates angiogenic protein levels in women with breast cancer receiving tamoxifen therapy, Cts-Clin. Transl. Sci. 6 (2013) 386–390.
[20] P. Moreau, A.A. Chanan-Khan, A.W. Roberts, A.B. Agarwal, T. Facon, S. Kumar, et al., Venetoclax combined with bortezomib and dexamethasone for patients with relapsed/refractory multiple myeloma, Blood 128 (2016).
[21] H. Wang, M. Li, J.J. Rinehart, R.W. Zhang, Pretreatment with dexamethasone increases antitumor activity of carboplatin and gemcitabine in mice bearing human cancer xenografts: in vivo activity, pharmacokinetics, and clinical implications for cancer chemotherapy, Clin. Cancer Res. 10 (2004) 1633–1644.
[22] M. Leggas, K.L. Kuo, F. Robert, G. Cloud, M. Deshazo, R.W. Zhang, et al., Intensive anti-inflammatory therapy with dexamethasone in patients with non-small cell lung cancer: effect on chemotherapy toxicity and efficacy, Cancer Chemother. Pharmacol. 63 (2009) 731–743.
[23] J.D. Martin, M. Panagi, C. Wang, T.T. Khan, M.R. Martin, C. Voutouri, et al., Dexamethasone increases cisplatin-loaded nanocarrier delivery and efficacy in metastatic breast cancer by normalizing the tumor microenvironment, ACS Nano 13 (2019) 6396–6408.
[24] A.M. Alessandro Poggi, Silvia Boero, Paolo Canevali, Maria Raffaella Zocchi, Statins as either immunomodulators or anti-cancer drugs: functional activities on tumor stromal cells and natural killer cells, Anti-Inflamm. Anti-Allergy Agents Med. Chem. 9 (2010) 82–92.
[25] T.V. Perneger, P.K. Whelton, M.J. Klag, Risk OF kidney failure associated with the use OF acetaminophen, aspirin, and nonsteroidal antiinflammatory drugs, N. Engl. J. Med. 331 (1994) 1675–1679.
[26] D. Liu, A. Ahmet, L. Ward, P. Krishnamoorthy, E.D. Mandelcorn, R. Leigh, et al., A practical guide to the monitoring and management of the complications of systemic corticosteroid therapy, Allergy Asthma Clin. Immunol. 9 (2013).
[27] L.A.G. Rodriguez, H. Jick, Risk OF upper gastrointestinal-bleeding and perforation associated with individual nonsteroidal antiinflammatory drugs, Lancet 343 (1994) 769–772.
[28] P.-Y. Chuang, S.-H. Shen, T.-Y. Yang, T.-W. Huang, K.-C. Huang, Non-steroidal anti-inflammatory drugs and the risk of a second hip fracture: a propensity-score matching study, BMC Muscoskelet. Disord. 17 (2016).
[29] L.J. Scully, D. Clarke, R.J. Barr, Diclofenac induced hepatitis - 3 cases with features OF autoimmune chronic active hepatitis, Dig. Dis. Sci. 38 (1993) 744–751.
[30] P. Ungprasert, N. Srivali, K. Wijarnpreecha, P. Charoenpong, E.L. Knight, Non-steroidal anti-inflammatory drugs and risk of venous thromboembolism: a systematic review and meta-analysis, Rheumatology 54 (2015) 736–742.
[31] W. Song, Z. Tang, D. Zhang, Y. Zhang, H. Yu, M. Li, et al., Anti-tumor efficacy of c (RGDfK)-decorated polypeptide-based micelles co-loaded with docetaxel and cisplatin, Biomaterials 35 (2014) 3005–3014.
[32] N-j Song, L-j Zhou, W-k Liu, X-l He, Z-c Pan, M-m Ding, et al., Effect of trastuzumab on the micellization properties, endocytic pathways and antitumor activities of polyurethane-based drug delivery system, Chin. J. Polym. Sci. 35 (2017) 909–923.
[33] M. Li, Z. Tang, D. Zhang, H. Sun, H. Liu, Y. Zhang, et al., Doxorubicin-loaded polysaccharide nanoparticles suppress the growth of murine colorectal carcinoma and inhibit the metastasis of murine mammary carcinoma in rodent models, Biomaterials 51 (2015) 161–172.
[34] Q. Wang, Y. Li, X. Chen, H. Jiang, Z. Zhang, X. Sun, Optimized in vivo performance of acid-liable micelles for the treatment of rheumatoid arthritis by one single injection, Nano Res. 12 (2019) 421–428.
[35] H. Guo, C-l Yang, W. Wang, Y-k Wu, Q-y Lai, Z. Yuan, Studies on antineoplastic effect by adjusting ratios of targeted-ligand and antitumor drug, Chin. J. Polym. Sci. 32 (2014) 540–550.
[36] W. Shen, W. Liu, H. Yang, P. Zhang, C. Xiao, X. Chen, A glutathione-responsive sulfur dioxide polymer prodrug as a nanocarrier for combating drug-resistance in cancer chemotherapy, Biomaterials 178 (2018) 706–719.
[37] X. Feng, W. Xu, Z. Li, W. Song, J. Ding, X. Chen, Immunomodulatory Nanosystems. Advanced Science vol. 6, Baden-Wurttemberg, Germany), Weinheim, 2019, p. 1900101.
[38] Q.X. Sun, M. Barz, B.G. De Geest, M. Diken, W.E. Hennink, F. Kiessling, et al., Nanomedicine and macroscale materials in immuno-oncology, Chem. Soc. Rev. 48 (2019) 351–381.
[39] Y. Shi, T. Lammers, Combining nanomedicine and immunotherapy, Acc. Chem. Res. 52 (2019) 1543–1554.
[40] W. Song, S.N. Musetti, L. Huang, Nanomaterials for cancer immunotherapy, Biomaterials 148 (2017) 16–30.
[41] S. Li, X. Feng, J. Wang, W. Xu, M.A. Islam, T. Sun, et al., Multiantigenic nanoformulations activate anticancer immunity depending on size, Adv. Funct. Mater. 29 (49) (2019).
[42] S. Li, X. Feng, J. Wang, L. He, C. Wang, J. Ding, et al., Polymer nanoparticles as adjuvants in cancer immunotherapy, Nano Res. 11 (2018) 5769–5786.
[43] P. Agarwalla, S. Mukherjee, B. Sreedhar, R. Banerjee, Glucocorticoid receptor-mediated delivery of nano gold-withaferin conjugates for reversal of epithelial-to-mesenchymal transition and tumor regression, Nanomedicine 11 (2016) 2529–2546.
[44] Q. Dong, X. Wang, X. Hu, L. Xiao, L. Zhang, L. Song, et al., Simultaneous application of photothermal therapy and an anti-inflammatory prodrug using pyrene-aspirin-loaded gold nanorod graphitic nanocapsules, Angew. Chem. Int. Ed. 57 (2018) 177–181.
[45] R.K. Pathak, S. Marrache, J.H. Choi, T.B. Berding, S. Dhar, The prodrug platin-A: simultaneous release of cisplatin and aspirin, Angew. Chem. Int. Ed. 53 (2014) 1963–1967.
[46] M. Coimbra, C.J.F. Rijcken, M. Stigter, W.E. Hennink, G. Storm, R.M. Schiffelers, Antitumor efficacy of dexamethasone-loaded core-crosslinked polymeric micelles, J. Control. Release 163 (2012) 361–367.
[47] L. Shi, L. Xu, C. Wu, B. Xue, X. Jin, J. Yang, et al., Celecoxib-induced self-assembly of smart albumin-doxorubicin conjugate for enhanced cancer therapy, ACS Appl. Mater. Interfaces 10 (2018) 8555–8565.
[48] S. Lv, Z. Tang, D. Zhang, W. Song, M. Li, J. Lin, et al., Well-defined polymer-drug conjugate engineered with redox and pH-sensitive release mechanism for efficient delivery of paclitaxel, J. Control. Release 194 (2014) 220–227.
[49] Z. Song, Z. Han, S. Lv, C. Chen, L. Chen, L. Yin, et al., Synthetic polypeptides: from polymer design to supramolecular assembly and biomedical application, Chem. Soc.

Rev. 46 (2017) 6570–6599.
[50] Q. Xu, Z. Zhang, C. Xiao, C. He, X. Chen, Injectable polypeptide hydrogel as biomimetic scaffolds with tunable bioactivity and controllable cell adhesion, Biomacromolecules 18 (2017) 1411–1418.
[51] S. Lv, Y. Wu, K. Cai, H. He, Y. Li, M. Lan, et al., High drug loading and sub-quantitative loading efficiency of polymeric micelles driven by donor-receptor coordination interactions, J. Am. Chem. Soc. 140 (2018) 1235–1238.
[52] S. Lv, Z. Tang, M. Li, J. Lin, W. Song, H. Liu, et al., Co-delivery of doxorubicin and paclitaxel by PEG-polypeptide nanovehicle for the treatment of non-small cell lung cancer, Biomaterials 35 (2014) 6118–6129.
[53] M-t Wang, Y. Jin, Y-x Yang, C-y Zhao, H-y Yang, X-f Xu, et al., In vivo biodistribution, anti-inflammatory, and hepatoprotective effects of liver targeting dexamethasone acetate loaded nanostructured lipid carrier system, Int. J. Nanomed. 5 (2010) 487–497.
[54] Y. Zhang, M. Huo, J. Zhou, S. Xie, PKSolver: an add-in program for pharmacokinetic and pharmacodynamic data analysis in microsoft excel, Comput. Methods Progr. Biomed. 99 (2010) 306–314.
[55] W. Song, L. Shen, Y. Wang, Q. Liu, T.J. Goodwin, J. Li, et al., Synergistic and low adverse effect cancer immunotherapy by immunogenic chemotherapy and locally expressed PD-L1 trap, Nat. Commun. 9 (2018).
[56] E.A. Sykes, J. Chen, G. Zheng, W.C.W. Chan, Investigating the impact of nanoparticle size on active and passive tumor targeting efficiency, ACS Nano 8 (2014) 5696–5706.
[57] Y. Wang, W. Song, M. Hu, S. An, L. Xu, J. Li, et al., Nanoparticle-mediated HMGA1 silencing promotes lymphocyte infiltration and boosts checkpoint blockade immunotherapy for cancer, Adv. Funct. Mater. 28 (2018).
[58] W. Song, M. Das, Y. Xu, X. Si, Y. Zhang, Z. Tang, et al., Leveraging biomaterials for cancer immunotherapy: targeting pattern recognition receptors, Materials Today Nano 5 (2019) 100029.
[59] Q. Chen, L. Feng, J. Liu, W. Zhu, Z. Dong, Y. Wu, et al., Intelligent albumin-MnO2 nanoparticles as pH-/H2O2-responsive dissociable nanocarriers to modulate tumor hypoxia for effective combination therapy (vol 28, pg 7129, 2016), Adv. Mater. 30 (2018).
[60] S. Zelenay, A.G. van der Veen, J.P. Boettcher, K.J. Snelgrove, N. Rogers, S.E. Acton, et al., Cyclooxygenase-dependent tumor growth through evasion of immunity, Cell 162 (2015) 1257–1270.
[61] M. Lasa, M. Brook, J. Saklatvala, A.R. Clark, Dexamethasone destabilizes cyclooxygenase 2 mRNA by inhibiting mitogen-activated protein kinase p38, Mol. Cell. Biol. 21 (2001) 771–780.